Using Light-Induced Thermocleavage in a Roll-to-Roll Process for Polymer Solar Cells†

Frederik C. Krebs* and Kion Norrman

Risø National Laboratory for Sustainable Energy, Technical University of Denmark, Frederiksborgvej 399, DK-4000 Roskilde, Denmark

ABSTRACT We report on the use of intense visible light with a narrow spectral distribution matched to the region where the conjugated polymer material absorbs to selectively heat the active material and induce thermocleavage. We show a full roll-to-roll process, leading to complete large-area polymer solar cell modules using light-induced thermocleavage. The process employs full solution processing in air for all five layers in the device and does not employ indium–tin oxide or vacuum processing. The process steps were carefully analyzed using X-ray photoelectron spectroscopy, time-of-flight secondary ion mass spectrometry, attenuated total reflectance infrared, and transmission/reflection UV–vis techniques.

KEYWORDS: thermocleavable materials • light-induced cleavage • laser light cleavage • indium–tin oxide free • vacuum free • polymer solar cells • organic photovoltaics (OPV)

INTRODUCTION

Polymer solar cells distinguish themselves from all other photovoltaic technologies in their diversity. They typically comprise a multilayer structure that can be prepared from a near-limitless combination of materials using a wide combination of coating and printing techniques (1–9). In addition, the multilayer structure (or a part of it) may be processed in a particular manner during or after formation. The traditional processing techniques have involved thermal annealing, solvent annealing, or slow drying. All of these operations have in common that they alter the film morphology and nanostructure in a way that is beneficial for device function. Currently, there are few approaches to stabilize and control the nanomorphology (10, 11). In addition to the early precursor routes (12–18) and the more recent thiocarbamate precursor route (19–23), a relatively novel class of materials have been developed that offer a new processing dimension in addition to that mentioned above in that it is possible to alter the chemistry and thereby also the physical properties of the materials via a heating step (24–37). The prototypical example is poly[3-(2-methylhex-2-yl)oxycarbonyldithiophene] (P3MHOCT) (24), which is a soluble polymer akin to poly(3-hexylthiophene) (P3HT). Upon heating, it eliminates an alkene to give poly(3-carboxydithiophene) (P3CT), which is insoluble in organic solvents (Scheme 1).

Further heating gives native polythiophene (PT) (26). Not only has this approach made it possible to reach three different chemical states for the same precursor film, it has also enabled solution processing of native PT, which historically has been an intractable material. Power conversion efficiencies of up to 1.5% for devices based on a bulk heterojunction of native PT and [70]PCBM have been reached as reported earlier (10). One drawback is the relatively high temperatures that are required for thermocleavage (~200 °C). The temperature of thermocleavage can be lowered (~130 °C) by using acid catalysis in conjunction with tetrahydropyran side groups, in which case an alcohol remains on the polymer backbone (36). In the context of polymer solar cells, these high processing temperatures pose a significant challenge if one is to envisage high-volume, high-speed manufacture on low-cost flexible substrates such as poly(ethylene terephthalate) (PET) that will endure only 140 °C without significant deformation. This was explored in the industrial manufacture and first large-scale public demonstration of polymer solar cells (38), where thermocleavage of P3MHOCT on PET at 140 °C was carried out by long heating times. P3MHOCT does thermocleave at 140 °C, while the reaction is very slow and 4 h was required to achieve insolubility of the active layer. The long period of time required for thermocleavage was a significant limitation to the previous work, and while thermocleavable materials offer a new processing dimension (film chemistry), new methods for achieving thermocleavage are needed. The limited use of thermocleavable polymer materials in the context of polymer solar cells may, in addition, be due to

Scheme 1. Reaction Scheme Showing the Transformation of P3MHOCT to P3CT at ~200 °C and P3CT to PT at ~300 °C

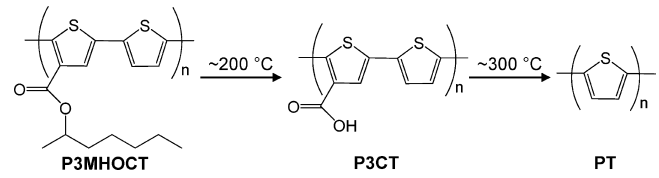

† A patent application covering the inventions described in this article has been filed.

* E-mail: frkr@risoe.dtu.dk.

Received for review December 4, 2009 and accepted February 16, 2010

DOI: 10.1021/am900858x

their complex synthetic makeup as compared to commonly employed polymer materials.

In this work, high-intensity visible light within a narrow-wavelength range was explored as a new method for selectively heating the thermocleavable layer to achieve fast thermocleavage in a full roll-to-roll process on flexible plastic substrates. The thermocleavage reaction was studied by the chemical characterization techniques time-of-flight secondary ion mass spectrometry (TOF-SIMS) and X-ray photoelectron spectroscopy (XPS) to ascertain the chemical transformations and the lateral distribution of materials in the device. Large-area polymer solar cell modules were prepared entirely by the solution processing of five layers using light for thermocleavage. Different substrate materials with varying thermal stability were explored. All preparative steps were performed in air by solution printing or coating.

EXPERIMENTAL SECTION

Materials. All solvents were standard grade. P3MHOCT was prepared and purified according to the literature (24, 38–41). The polymer had the following characteristics after purification: $M_n = 11\,300$, $M_w = 36\,900$, $M_p = 29\,800$, and polydispersity = 3.3. PCBM was purchased from Solenne BV with a purity of 99%. The active materials were dissolved in a 1:1 mixture of 1,2-dichlorobenzene and chloroform to procure the inks. The concentrations were as follows: P3MHOCT (22 mg mL^{-1}) and PCBM (22 mg mL^{-1}). Poly(3,4-ethylenedioxythiophene)–poly(styrenesulfonate) (PEDOT–PSS) was purchased from Agfa (Orgacon EL-P 5010) and diluted with isopropyl alcohol prior to use such that the viscosity reached 270 mPa · s at a temperature of 18 °C. A dispersion of ZnO nanoparticles was prepared as described earlier (42). Silver nanoparticle solutions for the silver back electrode were prepared as described earlier (43), and the silver employed for the grid front electrode was purchased from Dupont (PV410). The polyimide substrate (Kapton) was purchased from Skultuna Flexibles and had a web width of 290 mm and a thickness of 125 μm.

Roll-to-Roll Coating and Printing. Two roll-to-roll coating systems were employed. The first one was for slot-die coating, which employs a coating of liquid ink by pumping it through a coating head with slots where the ink exit and is applied to the substrate. The second one was for screen printing. The slot-die coating system comprised an unwinder, corona treater (electric discharge ionizes the surface of the foil), edge guide, cleaning station, coating roller, hot-air oven (1 m length, 140 °C), cooling roller, and winding station (42). The screen printing system comprised an unwinder, camera-controlled registration system, vacuum table, printer, hot-air oven (1.2 m length, 120 °C), transport roller, tensioning roller, and winding station. The process started by the coating of silver nanoparticles, where the polyimide substrate was corona-treated at a power of 1080 W and subsequently cleaned for dust using a double-sided cleaning system from Teknek, employing a static discharge rod immediately following the cleaning station and a second one immediately before the coating roller (20 cm).

The back electrode was prepared by the coating of silver nanoparticles as either 16 × 13 mm wide stripes spaced by 2 mm or as described earlier (43) as 8 × 9, 3 × 9, and 2 × 9 mm spaced by 3 mm and a single 9 mm stripe (42, 44). This gave the possibility to make single cells and modules with up to 16 serially connected stripes as shown in Figure 1, where the 16 coated silver stripes with 13 mm width run along the entire length of the roll (Figure 1A,B). The printed silver grid electrodes are 6 cm long and make the serial connection between the stripes in the final printing step (Figure 1C,D). The silver

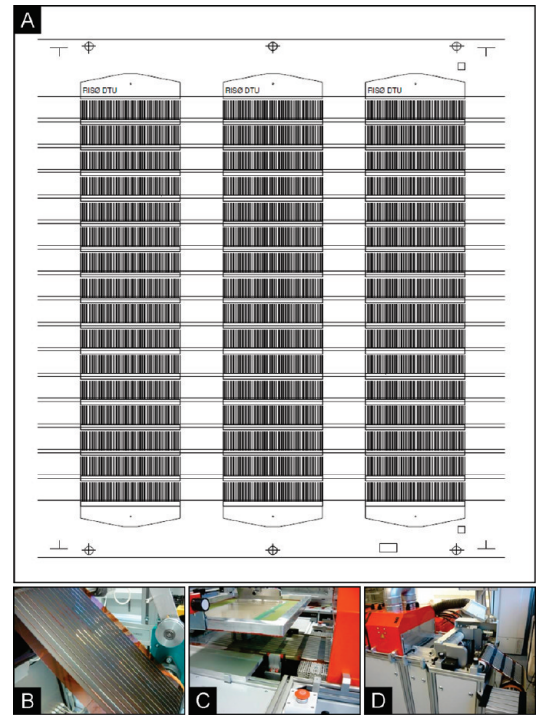

FIGURE 1. (A) Silver stripes are shown along the web direction along with an overlay of the printed silver grid electrode. Three silver cells measuring 6 cm in length along the web direction were printed simultaneously. (B) Kapton foil with 16 stripes after coating of PEDOT–PSS. (C) Screen printing of the silver electrode. (D) Rewinding of the completed modules.

nanoparticle solution was slot-die-coated at a speed of 1 m min^{-1} and dried with an oven temperature of 140 °C, giving a reflective silver electrode with a sheet resistivity of 0.02–0.03 $\Omega\,\square^{-1}$. During printing of the silver, each module was labeled using an inline ink-jet printer. Subsequently, two layers of zinc oxide were slot-die-coated (vide supra) at a speed of 2 m min^{-1} to limit the presence of shorts. The active layer was, subsequently, slot-die-coated at a speed of 1.4 m min^{-1} (P3MHOCT–PCBM). The material was cleaved using light (see section 2.3) prior to slot-die coating of the PEDOT–PSS solution at a speed of 0.2–0.4 m min^{-1}. The solar cell modules were completed by screen printing of the silver grid front electrode. Following screen printing of the electrodes, the modules were encapsulated in a full roll-to-roll process using an ultra barrier material from Alcan packaging as described earlier (45). The devices were then complete and ready for characterization.

Light-Cleaving Apparatus, Dose Determination, and R2R-Coated Light-Induced Thermocleaving. A diode array comprising 182 lines of 7 serially connected high-power light-emitting diodes (LEDs) were wire bonded onto a silver-plated copper bar. A total of 1274 LED chips were mounted on an area measuring 273.5 × 11 mm^2. The LED array was protected by a thin layer of silicone that was sealed with a 0.5-mm-thick glass plate. The distance from the LED chip to the surface of the glass was 1 mm. The copper bar with the array was mounted on an aluminum cooling plate (see Figure 2). The nominal forward current through the device was 64 A/25 V = 1.6 kW. The array could be pulsed with a ~33% duty cycle up to 200 A/30 V = 6 kW_{peak} without problems. The nominal optical output was 234 W at a wavelength of 460 nm with a full-width at half-maximum (fwhm) bandwidth of 20 nm (see Figure 2). During operation in pulsed mode, an optical output of approximately 700 W_{peak} could be reached. The power density at the surface of the array was 7.8 W cm^{-2} and 23 W_{peak} cm^{-2} using respectively normal and pulsed drive power. Because of the efficient water cooling,

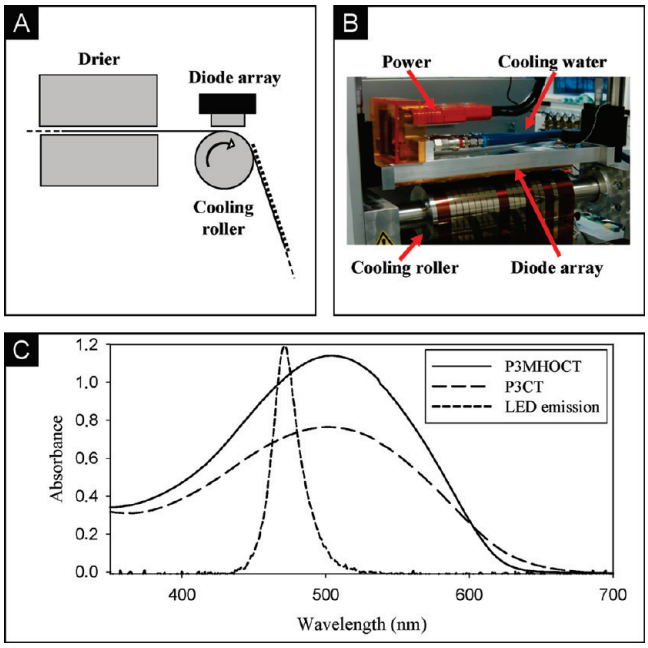

FIGURE 2. (a) Schematic drawing of the setup and (b) a photograph of the water-cooled diode array over the cooling roller. (c) Absorption spectra of P3MHOCT and P3CT along with the emission spectrum of the diode array.

the system could be operated for hours at 15 W cm^{-2} and for a short duration (15 min) at 23 W cm^{-2}. The dose of light required for thermocleavage was determined using a laser light. An approximately 100-nm-thick P3MHOCT film was spin-coated onto a substrate consisting of a 130-μm-thick PET film with a 75-nm-thick layer of indium−tin oxide (ITO). The film absorbance was around 1 for a 100-nm-thick film of pure P3MHOCT. The P3MHOCT film on the substrate was mounted in a holder for illumination. Illumination was carried out using a diode-pumped Nd:YAG laser of 532 nm wavelength and having a maximum output power of 4.9 W. One 25 ms pulse with a spot size of 0.625 mm (resulting in an energy delivery to the layer of approximately 40 J cm^{-2}) was delivered manually using an acousto-optic modulator, which was sufficient to convert P3MHOCT through the entire 100 nm film to P3CT. Conversion of P3MHOCT to P3CT was determined by rubbing the polymer film with a cotton bud soaked in chlorobenzene. The fully converted film remained insoluble in the solvent, whereas the unconverted or partially converted film was soluble in the solvent and was seen as a red coloring on the cotton bud. The conversion was also confirmed by observation of the infrared (IR) spectrum of the film using attenuated total reflectance IR (ATR-IR). Illumination under the same conditions but using a single pulse with a duration of 100 ms, giving approximately 160 J cm^{-2}, resulted in conversion to PT. Conversion to PT was determined by observation of the IR spectrum of the film; the IR spectrum of PT does not contain a C═O stretch at ca. 1700 cm^{-1}, whereas this peak is present in the spectrum of P3CT.

The device films with the coating of the soluble active layer were thermocleaved using the diode array at web speeds of 0.2−0.4 m min^{-2}. The energy density delivered to the surface of the film was between 70 and 12 J cm^{-2}. The fastest speed possible where insolubility was reached was around 0.3 m min^{-1}, while partial solubility (and thermocleavage) was reached at speeds of 0.2−0.4 m min^{-1} (depending on the power setting). At higher speeds, no thermocleavage was observed.

TOF-SIMS, XPS, and Atomic Force Microscopy (AFM) Analysis. TOF-SIMS analysis was performed using a TOF-SIMS IV (ION-TOF GmbH, Münster, Germany). Pulses of 15 ns of 25 keV Bi^+ (primary ions) were bunched to form ion packets with a nominal temporal extent of <0.9 ns at a repetition rate of 10 kHz, yielding a target current of 0.9 pA. These primary ion conditions were used to scan a 500 × 500 μm^2 area of the sample for 328 s. Electron bombardment (20 eV) was used to minimize charge built up at the surface. Desorbed secondary ions were accelerated to 2 keV, mass analyzed in the flight tube, and postaccelerated to 10 keV before detection.

XPS analyses were performed on a Kα (Thermo Electron Limited, Winsford, U.K.) using a monochromated Al Kα X-ray source and a takeoff angle of 90° from the surface plane. Atomic concentrations were determined from surface spectra (0−1350 eV, 200 eV detector pass energy) and were calculated by determining the relevant integral peak intensities using a Shirley-type background. High-resolution C_{1s} spectra were acquired with a detector pass energy of 25 eV. AFM imaging was performed on a N8 NEOS (Bruker Nano GmbH, Herzogenrath, Germany) operating in intermittent contact mode and using SSS-NCLR cantilevers (NANOSENSORS, Neuchatel, Switzerland). Images were recorded at a scan speed of 0.1 lines min^{-1}.

Solar Cell Characterization. The solar cell modules were characterized using a solar simulator from Steuernagel Lichttechnik (KHS 575). The solar simulator was calibrated using a bolometric pyranometer from Eppley Laboratories, and the spectral distribution was checked with an Avaspec-2048 from Avantes. The conditions were AM1.5G, 1000 W m^{-2}, and 72 °C.

RESULTS AND DISCUSSION

Thermocleavable Materials and Substrates for Roll-to-Roll Coating of Organic Photovoltaics (OPV). Thermocleavable materials (12–38) are soluble and can be processed into a thin film using common film-forming techniques. After thermal treatment, some of the material is eliminated, leaving the desired functional film insoluble. Two classes of thermocleavable materials for polymer solar cells are available. One class is thermocleavable through a precursor route (12–23), where the conjugated polymer backbone is formed during the thermal heating step and the other class has a conjugated polymer backbone bearing thermocleavable solubilizing side chains (24–38). Examples of the precursor route are the prototypical Wessling (12–15) and Durham (16–18) routes and the more recent dithiocarbamate route (19–23). The route employing thermocleavable side chains is so far limited to the Chugaev-type elimination reaction of esters and carbonates. Both methods have been explored in the context of polymer solar cells, and while the goal of pursuing these routes is to achieve advantages in processing and device stability, one drawback has been a relatively poor performance of solar cell devices. Recently, efficiencies approaching 2% have been reported for thermocleavable materials based on the thermocleavable side-chain route (10). The difficulty in achieving a high-power conversion efficiency that approaches the state-of-the-art seems to be the challenge associated with the thermal processing. In addition to the morphological changes induced by heating of the active material during thermocleavage, one also introduces a new dimension of chemistry in the film. It is possible to partially or fully change the chemical state of the film, and in some cases, several chemical states are reachable from the same precursor film (10, 26). IR laser light has been reported for

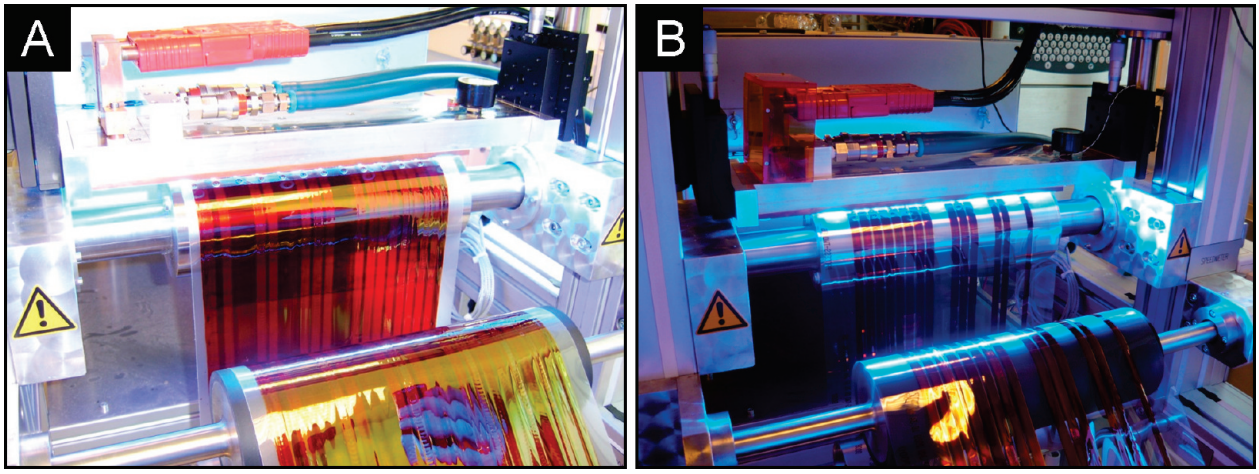

FIGURE 3. (a) Light cleaving of knife-coated P3MHOCT on PET by illumination through a Teflon mask. Notice that the undulations due to pulsing in the cleaved area have the lighter color. (b) When slot-die-coated stripes of P3MHOCT were cleaved on slot-die-coated silver stripes using PEN as the substrate, no undulations were observed. Both photographs were taken during a light pulse.

use of the thermocleavage and patterning of a conjugated polymer based on thermocleavable side chains (35, 37).

In the context of this work, which employs visible light in a wavelength region where the conjugated polymer material absorbs the class of materials, most relevant are the conjugated materials bearing solubilizing side chains. Materials for the precursor route would also work in this case, where the substrate absorbs the wavelengths of light employed or by inclusion of absorber materials. The precursor route would possibly not be applicable in cases where a transparent substrate is employed because the absorption of the precursor polymer is normally in the UV region, where high-power LED sources are less readily available. One challenge associated with both classes of materials is the relatively high temperature required for thermocleavage. In the case of P3MHOCT, thermocleavage to P3CT takes place at ~200 °C, and further thermocleavage to PT takes place at ~300 °C (26). Most relevant plastic substrates for polymer solar cells will not support these temperatures. As examples, relevant low-cost transparent plastic substrates such as the biodegradable poly(lactic acid) (PLA), PET, and poly(ethylene naphthalenate) (PEN) support temperatures of respectively 65, 140, and 180 °C. Attempts were made to employ both PET and PEN for processing in this work, and while it was possible to achieve light-induced thermocleavage and even patterning, it was not practical because heating of the film leads to permanent deformation of the substrate. From this point of view, only heat-stable substrates are truly compatible with the process proposed here such as solid metal foils (46) and polymer substrates such as polyimide (Kapton). Both metal films and Kapton are, in contrast to PLA, PET, and PEN, not transparent or poorly transparent and thus require that the solar cell is processed from the backside.

Roll-to-Roll Coating of Polymer Solar Cells Using Full Solution Processing. The majority of polymer solar cells reported to date employ a transparent substrate (glass or PET) and a transparent electrode that is almost exclusively ITO. There have been some reports on devices employing transparent ITO-free electrodes that either consist of very high conductivity PEDOT (47) or a composite electrode of PEDOT—PSS and a silver grid (48–50). In the context of roll-to-roll coating of polymer solar cells, there have been relatively few reports and the most successful employ PET—ITO substrates (38, 42, 44, 45). Aside from the application of ITO through a vacuum process, the rest of the route is solution-processed, covering wet patterning and etching of the ITO, coating of the active layers, and printing of the back electrode, giving large modules with power conversion efficiencies ranging from very low (38) and up to 2.3% (44). There have been very few reports on roll-to-roll-compatible or roll-to-roll-coated polymer solar cells, where there is no requirement for the substrate to be transparent. In those reported cases, it should be noted that the processes are ITO-free, which is considered to be a great advantage (43, 46, 51). They cover the wrap-through concept (51), printed metallic back electrodes (ProcessTwo) (43), and metal foil back electrodes (ProcessFour) (46).

Light Cleaving of the Active Layer. Initial attempts employed PET and PEN substrates. Several experiments were made, and it was found possible to illuminate knife-coated P3MHOCT layers through a Teflon mask, thus selectively creating the desired striped pattern. The uncleaved P3MHOCT could be washed off with chloroform, leaving stripes of cleaved P3CT as shown in Figure 3. This patterning procedure could have advantages but would require a washing step. Because stripes can be formed easily with slot-die coating, this striped type of patterning was not found to be an advantage in this work. The best results were obtained using a pulsed operation of the LED lamp (33% duty cycle at 200 A, ~23 W_{peak} cm^{-2}). The pulses are, however, clearly visible on the photograph as undulations in the area of the stripes and reflect melting and deformation of the PET substrate due to excessive heating. Without pulsing, the substrate simply melted.

This improved somewhat in the case where PEN was used as the substrate (Figure 3), in which smooth cleaved layers were formed. The PEN material, however, shrank in a direction perpendicular to the web because of the heating, and it was not possible to achieve registry when electrodes

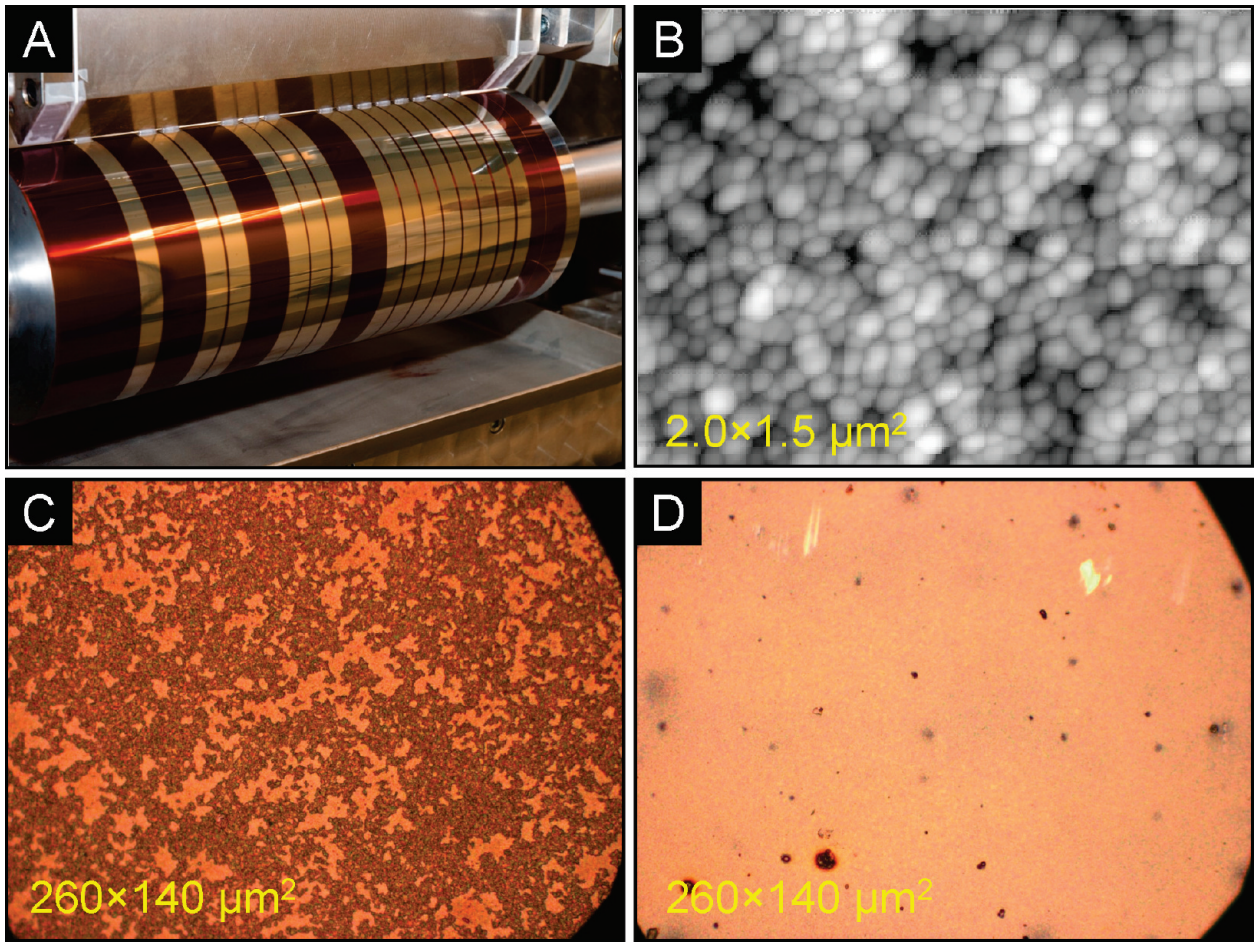

FIGURE 4. (A) Slot-die coating of the ZnO electrode on top of the slot-die-coated silver on Kapton. The meniscus of the ZnO solution is visible as a milky white solution. (B) AFM image of the silver nanoparticles. (C and D) Optical images of the ZnO layer using pure WS-1 as the solvent (C) and 20% WS-1 in *o*-xylene (D).

were printed at a later stage. It might be possible to take shrinkage into account during design of the patterns, but it was deemed impractical in the context of this work. It was clear that a very heat-stable substrate was required, and finally Kapton was chosen.

Characterization of the Coated Layers and the Extent of the Cleaving Process. The slot-die coating of the silver nanoparticles was more difficult on Kapton than on PEN. The adhesion was poorer, and the use of corona treatments did not improve the adhesion much, whereas wetting of the surface of Kapton with isopropyl alcohol immediately prior to coating improved the wettability and coating. ZnO nanoparticles were subsequently coated on top of the silver layer, and for the initial devices, it was found that most of the solar cells were short-circuited.

This was analyzed using both optical microscopy and AFM, and it was found that the ZnO ink based on WS-1 gave rise to large aggregates on the surface of the silver nanoparticle layer on Kapton (Figure 4C). The ZnO ink employed had been developed and used for coating on PET−ITO, and it was unexpected that this could lead to problems on Kapton and Kapton/silver. A different formulation in which the WS-1 content had been reduced to 20% by the addition of *o*-xylene gave smooth films (Figure 4D). This could possibly be a result of the different wetting and coating behavior of WS-1 on Kapton/silver, whereas the addition of *o*-xylene changes the wetting and coating behavior such that there is no dewetting during drying. The dewetting could be a result of the silicone impurities present on the surface of Kapton or in the silver ink. It was found using TOF-SIMS that there were some silicone impurities in the case of the ZnO/WS-$1_{100\%}$ ink, and in this case, silver was accessible from the surface, which could explain the observed short circuits (Figure 4B). Several experiments were made using the different inks and by coating of several layers using a combination of the inks. It was found that the ZnO/WS-$1_{100\%}$ ink gave rise to incomplete coverage, confirmed by the detection of silver using both XPS and TOF-SIMS (Figure 5). With coating using the ZnO/WS-$1_{20\%}$ ink, a covering layer was achieved on its own or by coating two layers of WS-$1_{20\%}$ on top of ZnO/WS-$1_{100\%}$ (Figure 5). A single layer on top was not enough to achieve complete coverage. Because of spectral overlap in the (quantitative) XPS spectra, it was not possible to quantify the low levels of silicone impurities using XPS, so the more sensitive (but only semiquantitative) technique TOF-SIMS was used to detect the silicone impurities. Silicone was detected on all sample surfaces, with ZnO/WS-$1_{100\%}$ showing the relatively highest degree of silicone contents and ZnO/WS-$1_{20\%}$ showing the lowest degree of silicone contents. The probe depth of TOF-SIMS is only ~1

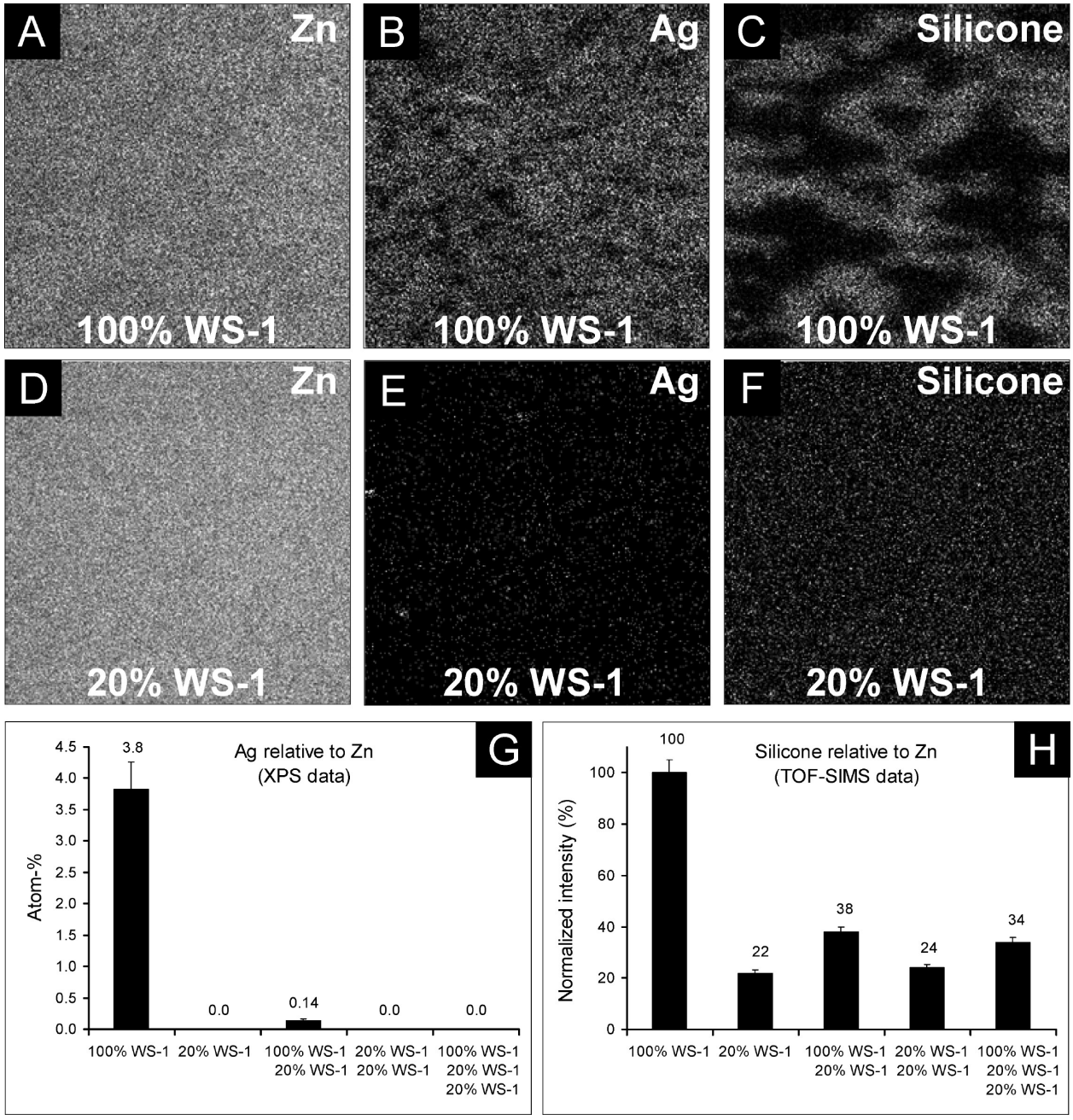

FIGURE 5. (A–F) TOF-SIMS images of the surfaces based on the ZnO/WS-$1_{100\%}$ ink (A–C) and the ZnO/WS-$1_{20\%}$ ink (D–F). Black corresponds to 0% signal, gray to some signal, and white to 100% signal. Silver is visible through the ZnO layer (B and E), and there are silicone impurities (C and F). XPS (G) and TOF-SIMS (H) measurements (average of 10 different surface locations) confirmed these findings. The mass spectral markers used were Zn^+, Ag^+, and $Si_2C_5H_{15}O^+$.

nm, so one would intuitively expect ZnO/WS-$1_{20\%}$ and ZnO/WS-$1_{100\%}$/WS-$1_{20\%}$ to show the same result with regard to silicone contents. This is, however, not the case; the two surfaces that contain a sublayer of WS-$1_{100\%}$ have elevated silicone contents. This is in each case believed to be due to silicone segregation from the sublayer of WS-$1_{100\%}$ to the outer surface of the upper layer of WS-$1_{20\%}$. The two surfaces containing a sublayer of WS-$1_{100\%}$ have more or less the same silicone contents, but on only one was silver detected (0.14 atom %).

This is not a surprising result; the XPS detection limit for silver is ~0.1 atom % (~1000 ppm); i.e., the silver content on ZnO/WS-$1_{100\%}$/WS-$1_{20\%}$/WS-$1_{20\%}$ is most likely just below the XPS detection limit. P3MHOCT was then slot-die-coated on top of the ZnO layer and thermocleaved using the LED array. The extent of the thermocleavage reaction was followed using XPS, which excellently demonstrated the capacity of the technique to gain good control of the extent of the reaction, and it was possible to process the P3MHOCT layer into P3CT or PT depending on the light intensity and web speed. The advantage of using XPS in this case is that it probes relatively deep into the surface of the film (~10 nm) and because P3MHOCT is fortuitously comprised of four distinct types of carbon, of which two are directly related to the extent of the reaction. The reaction is shown in Figure 6 where 0% reaction is defined as unreacted P3MHOCT, 50%

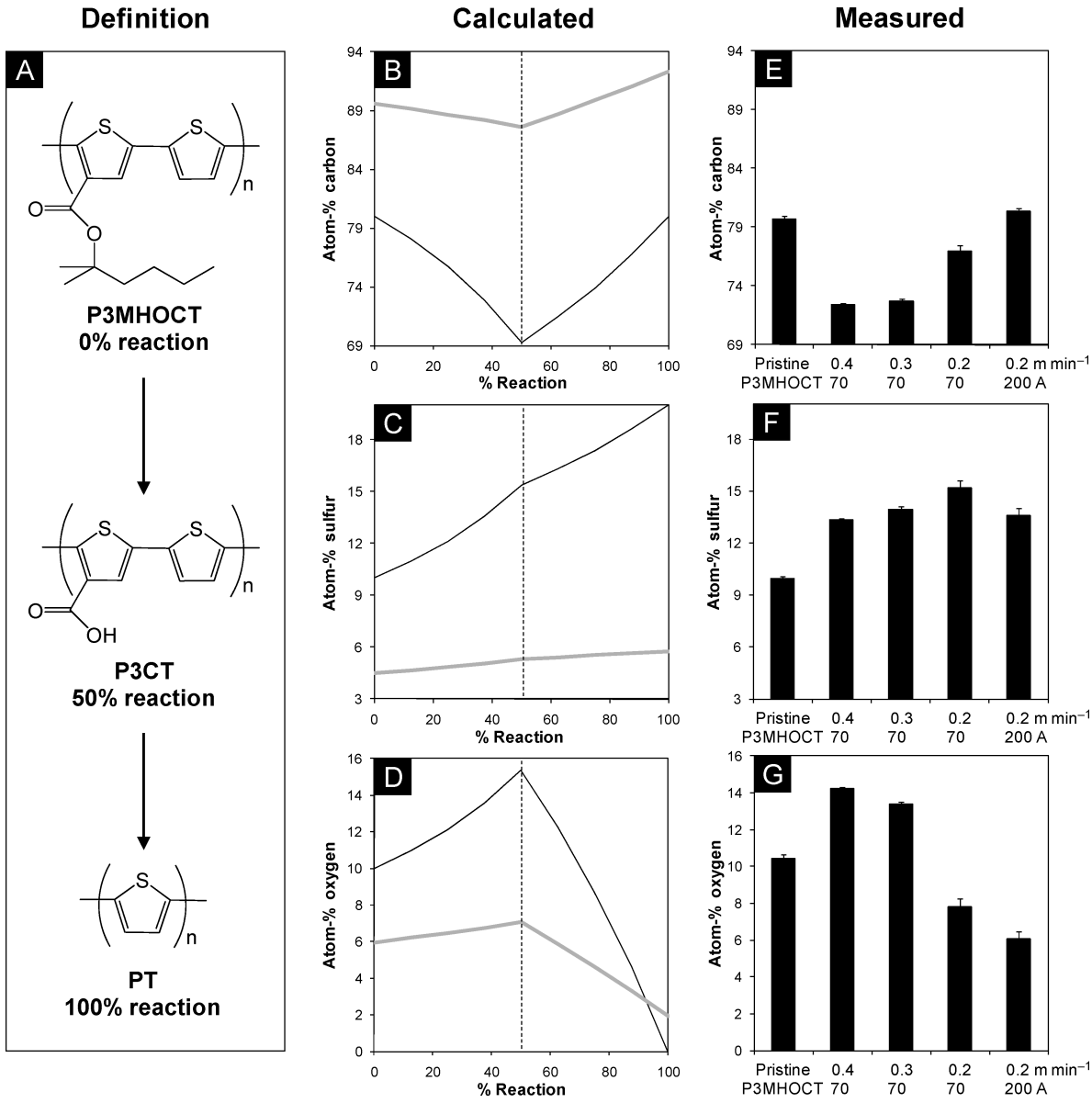

FIGURE 6. (A) Definition of the extent of the thermocleavage reaction starting from P3MHOCT through P3CT to PT. (B–D) Calculated distributions of carbon, oxygen, and sulfur compositions as a function of the extent of the thermocleavage reaction for pure P3MHOCT (black curve) and for a 1:1 mixture of P3MHOCT–PCBM (gray curve). (E–G) Experimentally determined carbon, oxygen, and sulfur compositions for various roll-to-roll illuminations of the Kapton/silver/ZnO/P3MHOCT–PCBM films as measured using XPS.

reaction is defined as complete conversion to P3CT, and 100% reaction is defined as complete conversion to PT. The observed atom percent correlates very well with the theoretical prediction except in the case of the sulfur and oxygen contents for PT. Ideally, the oxygen content should reach zero and the sulfur content should increase. This was, however, not observed. It is likely that the material partly oxidized during the relatively high temperature employed in an attempt to achieve 100% reaction. In order to investigate this further, a control experiment was performed using spin-coated samples of pure P3MHOCT and a 1:1 mixture of P3MHOCT–PCBM. The conversion of P3MHOCT and P3MHOCT–PCBM was carried out in a nitrogen atmosphere, and element compositions were measured by XPS and are listed in Table 1. Through a systematic comparison of the results, several interesting observations become evident. It appears that the R2R-fabricated P3MHOCT–PCBM sample has no detectable PCBM contents in the surface, a phenomenon well-known from P3HT–PCBM. However, the spin-coated P3MHOCT–PCBM sample contains PCBM in the surface, which becomes enriched on the PT–PCBM surface (revealed, e.g., by the sulfur contents), which explains the ~4 atom % oxygen compared to the ~2 atom % that was calculated. The PCBM enrichment is not observed for the R2R-produced PT–PCBM, so the ~6 atom % oxygen content must be due to oxygenation as a result of the relatively high temperature used during the conversion.

It should be stressed that these experiments were carried out in ambient air, and it is likely that photodegradation at high temperature comes into play and that either some of the sulfur is oxidized or the PT backbone is degraded. There are two main reasons for carrying out the experiments in air. First, the roll-to-roll coating equipment is large and difficult to enclose and operate in an

Table 1. XPS Data for the Model Devices at 0, 50, and 100% Reaction of P3MHOCT/P3CT/PT according to Figure [6] with and without PCBM[a]

	carbon (atom %)			sulfur (atom %)			oxygen (atom %)		
condition	R2R	model	calcd	R2R	model	calcd	R2R	model	calcd
P3MHOCT		80.3 ± 0.5	80.0		9.8 ± 0.3	10.0		9.9 ± 0.3	10.0
P3CT		71.7 ± 0.4	69.2		14.9 ± 0.2	15.4		13.5 ± 0.2	15.4
PT		79.2 ± 0.1	80.0		17.7 ± 0.3	20.0		3.1 ± 0.3	0.0
P3MHOCT−PCBM	79.7 ± 0.3	85.4 ± 0.0	89.6	10.0 ± 0.1	6.5 ± 0.2	4.5	10.4 ± 0.2	8.1 ± 0.3	6.0
P3CT-PCBM	72.7 ± 0.2	85.4 ± 0.5	87.6	13.9 ± 0.2	6.4 ± 0.2	5.3	13.4 ± 0.1	8.2 ± 0.3	7.1
PT-PCBM	80.4 ± 0.2	95.2 ± 0.3	92.3	13.6 ± 0.5	1.1 ± 0.2	5.8	6.1 ± 0.4	3.8 ± 0.1	1.9

[a] The conversion was carried out under an inert atmosphere to establish the extent of oxygen inclusion during the R2R light-cleaving experiment in air.

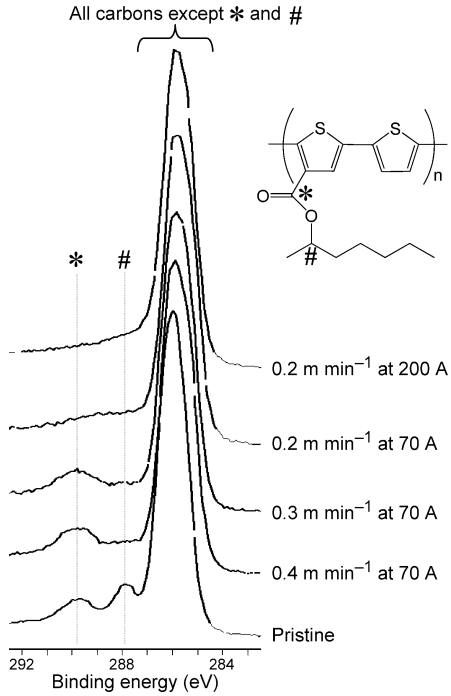

FIGURE 7. C_{1s} XPS spectra of Kapton/Ag/ZnO/P3MHOCT before (pristine) and after various degrees of light exposure, causing various degrees of thermocleavage. The degree of thermocleavage is monitored from the intensity of the peaks labeled # and *.

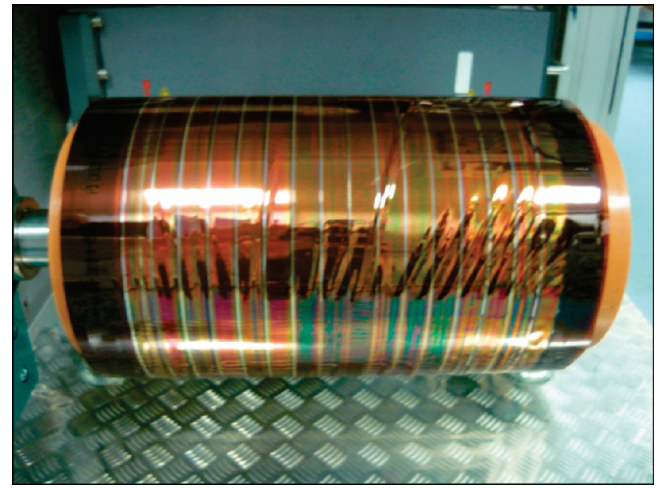

FIGURE 8. Photograph of the deformations observed in the region between cleaved and uncleaved materials. The LED-cleaved material is in the lower part of the image.

inert atmosphere. Second, there is an interest in developing the method such that it works under ambient conditions to reduce the cost and complexity to the minimum possible level. In Figure 7, XPS spectra are shown in the C_{1s} region along with a labeling of the different carbon atoms that comprise aromatic carbons in the thiophene rings, aliphatic CH_2 and CH_3 carbons, carbonyl carbons in the carboxylic acid/ester group, and alkoxy CHO carbons in the ester. The evolution is clear: when the film is subjected to continuous light from the diode array at 70 A and a web speed of 0.4 m min^{-1}, the aliphatic side chains are eliminated (partial loss of the peak labeled # in Figure 7), indicating an almost complete conversion to P3CT.

Upon a decrease of the web speed to 0.2 m min^{-1}, partial decarboxylation to PT was observed (partial loss of the peak labeled * in Figure 7), while upon a decrease in the web speed to 0.2 m min^{-1} and a tripling of the incident light intensity, complete conversion to PT is observed with some photoinduced or thermally induced oxidative degradation.

Completion and Performance of the Light-Cleaved Roll-to-Roll Coated Solar Cells. After light cleavage of the active layer, the devices were completed by slot-die-coating a layer of PEDOT−PSS, followed by screen printing of a silver grid electrode. The devices were encapsulated using a barrier material as described earlier. All of these processes were full roll-to-roll processes (42–46). It should be noted that while Kapton has excellent thermal stability (both chemical and mechanical), the thermocleavage of the thin overlying films did lead to deformations of the substrate. This is shown in Figure 8, where the material was light-cleaved and then the LED array was switched off. Deformations are observed in the region between cleaved and uncleaved materials. It should be noted that this observation was unique to Kapton and must be ascribed to its unique properties of thermal expansion. In the case of both PET and PEN, the deformations were not limited to the zone between cleaved and uncleaved materials but extended throughout the areas of the cleaved material. In terms of further processing of the LED-cleaved film, which includes slot-die coating of PEDOT−PSS and screen printing of silver on top of the cleaved film, it is important that the film does not deform such that coating and printing in

registry is still possible. With the deformations observed in the cases of PET and PEN, it was impossible to achieve coating and obtain registry after LED cleavage because the deformations were too extensive. The material shrank and was no longer planar, making it impossible to make complete devices.

In the case of Kapton, some deformation and shrinkage was observed (see Figure 8), but the material remained planar after LED cleavage, and it was only in the zone between cleaved and uncleaved materials that deformations were observed because of the shrinkage and the material was flat in the extended regions of light-cleaved material. One explanation for this could be that Kapton, which is a material with a significant optical absorption up to around 500 nm, is actually also heated by the LED illumination, and therefore heating is homogeneous throughout the illuminated area. In the cases of PET and PEN, only the regions that are coated with polymer absorb the LED light and are heated, whereas the regions between the stripes do not absorb and are thus not heated (or at least heated to a much lesser extent). The shrinkage was not prohibitive and amounted to 0.1 % and 0.6 % in the case of material cleaved to P3CT and PT, respectively. With the registration tolerance employed here (2 mm), this was not a problem over the width of the devices (260 mm).

This clearly will pose problems if one wishes to optimize the active area over the total area. In the device type explored below, the geometric fill factor was 67 % , and with the shrinkage observed, it is likely that the limit in the geometric fill factor that can be obtained is around 80−85 % when the same size of devices as those explored here are reported. In terms of performance, some devices were short-circuited as noted earlier (43). This was proposed to be due to silver short circuits, and this was confirmed in these experiments by the extensive XPS and TOF-SIMS analysis described previously. In terms of the photovoltaic performance, the devices performed as expected for devices prepared using ZnO with a dynamic IV behavior. When freshly prepared, the devices did not perform very well, but once illuminated and subjected to successive IV scans, the performance improved to a stable level as reported earlier (43–45). This typically took 5−25 min. The data presented in Figure 9 are thus annealed best-case devices. While the observed performance is significantly lower than the current state-of-the-art, it must be kept in mind that these devices are ITO-free and comprise five layers processed entirely from solution under ambient conditions. The trend observed on going from uncleaved P3MHOCT devices through devices light-cleaved to P3CT and further to PT follows roughly the expected behavior, as shown in Figure 9 and Table 2.

The thermocleavage of P3MHOCT−PCBM devices to P3CT−PCBM devices reduces the performance by a factor of about 3, followed by an increase to a similar level of performance when thermocleaving further to PT−PCBM, which corroborates with earlier findings (10). The overall performance is lower than that for devices prepared using P3HT−PCBM in the same device geometry by a factor of approximately 2. This is in rough agreement with a recent study where P3MHOCT−PCBM and PT−PCBM devices were studied and compared to P3HT−PCBM devices (52).

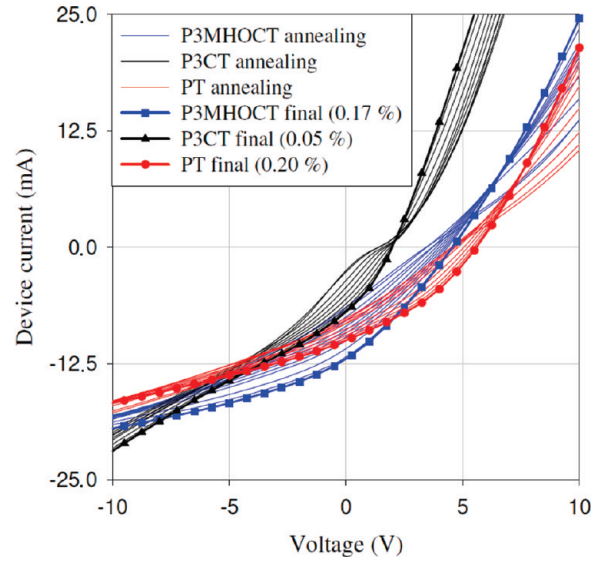

FIGURE 9. IV characteristics of the roll-to-roll-processed modules based on P3MHOCT, P3CT, and PT during annealing of the completed modules. The final performances after annealing are highlighted.

Table 2. Solar Cell Performance after Annealing (1000 W m^{-2}, AM1.5G, 85 ± 2 °C) according to Figure [9,a]

device	module V_{oc} (V)	module current (mA)	module FF (%)	P_{max} (mW)	module PCE (%)
P3MHOCT−PCBM	4.55	−11.99	29.7	16.2	0.17
P3CT−PCBM	1.97	−6.971	32.2	4.42	0.05
PT−PCBM	5.60	−10.00	34.6	19.4	0.20

[a] The maximum power and module PCE is given on the nominal active area for the entire module (96 cm^2).

Perspective and Outlook. In terms of power consumption, this method of heating has some advantages over a hot-air-drying system. In principle, thermocleavage can be achieved by passage through a hot-air drier, which is also available in the roll-coating system employed in this study. The advantage of the hot-air drier is simplicity in use, while the disadvantages are a high-power consumption and poor control of the web during heating (perhaps close to T_g of the substrate). The power usage employed here was typically around 1.6 kW for the high-power LED array, while the hot-air drier requires about 20 kW to reach 140 °C and 34 kW to reach 250 °C. The LED array has the advantage that the web is supported over the cooling roller and that the heated zone is limited to the width of the array (∼1 cm). In addition, it might be simpler to employ an inert atmosphere over the heated zone for the LED array even though it is difficult. The method described here would benefit from the possibility of creating shorter pulses with a higher power so as to selectively heat the active layer. This would enable the use of more heat-sensitive substrates such as PEN and PET and allow thermal processing of the active layer at temperatures well above the T_g of the substrate. The only technology

available for this currently is lasers, while this would seem to be too costly to be useful unless a CO_2 laser can be used. In terms of materials, clearly identifiable goals are to develop coatable silver inks that lead to smooth surfaces such that shorts are avoided entirely and to develop high-conductivity coatable electrodes with good optical transmission.

CONCLUSIONS

We successfully demonstrate a new roll-to-roll processing method whereby thermocleavable materials are heated selectively using a high-power LED source. We demonstrated that thermocleavable materials could be processed into different chemical states using intense LED light with a narrow bandwidth. We detailed the chemical changes in the films using surface-sensitive probes such as TOF-SIMS and XPS and further processed fully operational polymer solar cell modules. We showed the feasibility of the approach and identified several improvements that would need to be addressed efficiently before this approach can be expected to compete with the state-of-the-art. Those are, in turn, printable or coatable transparent electrodes with better optical transmission and better performing thermocleavable materials and methods to achieve thermocleavage at lower temperatures.

Acknowledgment. This work was supported by the Danish Strategic Research Council (Grants DSF 2104-05-0052 and 2104-07-0022). Jan Alstrup and Ole Hagemann are thanked for technical support. Lars Lindvold is gratefully acknowledged for aiding in the determination of the required dose using laser light. Torben Kjær is gratefully acknowledged for constructing the water-cooled LED array.

Supporting Information Available: Transmission UV—vis spectra of spin-coated films before and after washing with chlorobenzene, reflection UV—vis spectra of R2R-coated and light-processed P3MHOCT/P3CT/PT-PCBM films before and after washing with chlorobenzene, and ATR IR spectra of R2R-coated and light-processed P3MHOCT/P3CT/PT-PCBM films. The method for manufacture of polymer solar cells described in this work is known as ProcessThree. This material is available free of charge via the Internet at http://pubs.acs.org.

REFERENCES AND NOTES

(1) Günes, S.; Neugebauer, H.; Sariciftci, N. S. *Chem. Rev.* **2007**, *107*, 1324–1338.
(2) Bundgaard, E.; Krebs, F. C. *Sol. Energy Mater. Sol. Cells* **2007**, *91*, 954–985.
(3) Jørgensen, M.; Norrman, K.; Krebs, F. C. *Sol. Energy Mater. Sol. Cells* **2008**, *92*, 686–714.
(4) Thompson, B. C.; Fréchet, J. M. J. *Angew. Chem., Int. Ed.* **2008**, *47*, 58–77.
(5) Hadipour, A.; de Boer, B.; Blom, P. W. M. *Adv. Funct. Mater.* **2008**, *18*, 169–181.
(6) Ameri, T.; Dennler, G.; Lungenschmied, C.; Brabec, C. J. *Energy Environ. Sci.* **2009**, *2*, 347–363.
(7) Krebs, F. C. *Sol. Energy Mater. Sol. Cells* **2009**, *93*, 394–412.
(8) Dennler, G.; Scharber, M. C.; Brabec, C. J. *Adv. Mater.* **2009**, *21*, 1323–1338.
(9) Kippelen, B.; Brédas, J.-L. *Energy Environ. Sci.* **2009**, *2*, 251–261.
(10) Gevorgyan, S. A.; Krebs, F. C. *Chem. Mater.* **2008**, *20*, 4386–4390.
(11) Senkovskyy, V.; Tkachov, R.; Beryozkina, T.; Komber, H.; Oertel, U.; Horecha, M.; Bocharova, V.; Stamm, M.; Gevorgyan, S. A.; Krebs, F. C.; Kiriy, A. *J. Am. Chem. Soc.* **2009**, *131*, 16445–16453.
(12) Gagnon, D. R.; Capistran, J. D.; Karasz, F. E.; Lenz, R. W.; Antoun, S. *Polymer* **1987**, *28*, 567–573.
(13) Garay, R. O.; Mayer, B.; Karasz, F. E.; Lenz, R. W. *J. Polym. Sci., Part A: Polym. Chem.* **1995**, *33*, 525–531.
(14) Lenz, R. W.; Han, C. C.; Stengersmith, J.; Karasz, F. E. *J. Polym. Sci., Part A: Polym. Chem.* **1988**, *26*, 3241–3249.
(15) Wessling, R. A. *J. Polym. Sci., Polym. Symp.* **1985**, *72*, 55–66.
(16) Bott, D. C.; Brown, C. S.; Chai, C. K.; Walker, N. S.; Feast, W. J.; Foot, P. J. S.; Calvert, P. D.; Billingham, N. C.; Friend, R. H. *Synth. Met.* **1986**, *14*, 245–269.
(17) Feast, W. J.; Winter, J. N. *J. Chem. Soc., Chem. Commun.* **1985**, *4*, 202–203.
(18) Furlani, A.; Napoletano, C.; Russo, M. V.; Feast, W. J. *Polym. Bull.* **1986**, *16*, 311–317.
(19) Henckens, A.; Colladet, K.; Fourier, S.; Cleij, T. J.; Lutsen, L.; Gelan, J.; Vanderzande, D. *Macromolecules* **2005**, *38*, 19–26.
(20) Nguyen, L. H.; Gunes, S.; Neugebauer, H.; Sariciftci, N. S.; Banishoeib, F.; Henckens, A.; Cleij, T.; Lutsen, L.; Vanderzande, D. *Sol. Energy Mater. Sol. Cells* **2006**, *90*, 2815–2828.
(21) Banishoeib, F.; Adriaensens, P.; Berson, S.; Guillerez, S.; Douheret, O.; Manca, J.; Fourier, S.; Cleij, T. J.; Lutsen, L.; Vanderzande, D. *Sol. Energy Mater. Sol. Cells* **2007**, *91*, 1026–1034.
(22) Banishoeib, F.; Henckens, A.; Fourier, S.; Vanhooyland, G.; Breselge, M.; Manca, J.; Cleij, T. J.; Lutsen, L.; Vanderzande, D.; Nguyen, L. H.; Neugebauer, H.; Sariciftci, N. S. *Thin Solid Films* **2008**, *516*, 3978–3988.
(23) Girotto, C.; Cheyns, D.; Aernouts, T.; Banishoeib, F.; Lutsen, L.; Cleij, T. J.; Vanderzande, D.; Genoe, J.; Poortman, J.; Heremans, P. *Org. Electron.* **2008**, *9*, 740–746.
(24) Liu, J. S.; Kadnikova, E. N.; Liu, Y. X.; McGehee, M. D.; Fréchet, J. M. J. *J. Am. Chem. Soc.* **2004**, *126*, 9486–9487.
(25) Krebs, F. C.; Spanggaard, H. *Chem. Mater.* **2005**, *17*, 5235–5237.
(26) Bjerring, M.; Nielsen, J. S.; Nielsen, N. C.; Krebs, F. C. *Macromolecules* **2007**, *40*, 6012–6013.
(27) Krebs, F. C.; Norrman, K. *Prog. Photovoltaics: Res. Appl.* **2007**, *15*, 697–712.
(28) Bjerring, M.; Nielsen, J. S.; Siu, A.; Nielsen, N. C.; Krebs, F. C. *Sol. Energy Mater. Sol. Cells* **2008**, *92*, 772–784.
(29) Krebs, F. C. *Sol. Energy Mater. Sol. Cells* **2008**, *92*, 715–726.
(30) Krebs, F. C.; Thomann, Y.; Thomann, R.; Andreasen, J. W. *Nanotechnology* **2008**, *19*, 424013.
(31) Petersen, M. H.; Gevorgyan, S. A.; Krebs, F. C. *Macromolecules* **2008**, *41*, 8986–8994.
(32) Hagemann, O.; Bjerring, M.; Nielsen, N. C.; Krebs, F. C. *Sol. Energy Mater. Sol. Cells* **2008**, *92*, 1327–1335.
(33) Helgesen, M.; Gevorgyan, S. A.; Krebs, F. C.; Janssen, R. A. J. *Chem. Mater.* **2009**, *21*, 4669–4675.
(34) Yu, J. F.; Holdcroft, S. *Macromolecules* **2000**, *33*, 5073–5079.
(35) Gordon, T. J.; Yu, J. F.; Yang, C.; Holdcroft, S. *Chem. Mater.* **2007**, *19*, 2155–2161.
(36) Han, X.; Chen, X. W.; Holdcroft, S. *Adv. Mater.* **2007**, *19*, 1697–1702.
(37) Gordon, T. J.; Vamvounis, G.; Holdcroft, S. *Adv. Mater.* **2008**, *20*, 2486–2490.
(38) Krebs, F. C.; Jørgensen, M.; Norrman, K.; Hagemann, O.; Alstrup, J.; Nielsen, T.; Fyenbo, J.; Larsen, K.; Kristensen, J. *Sol. Energy Mater. Sol. Cells* **2009**, *93*, 422–441.
(39) Krebs, F. C.; Nyberg, R. B.; Jørgensen, M. *Chem. Mater.* **2004**, *16*, 1313–1318.
(40) Nielsen, K. T.; Bechgaard, K.; Krebs, F. C. *Macromolecules* **2005**, *38*, 658–659.
(41) Nielsen, K. T.; Bechgaard, K.; Krebs, F. C. *Synthesis* **2006**, 1639–1644.
(42) Krebs, F. C. *Sol. Energy Mater. Sol. Cells* **2009**, *93*, 465–475.
(43) Krebs, F. C. *Org. Electron.* **2009**, *10*, 761–768.
(44) Krebs, F. C.; Gevorgyan, S. A.; Alstrup, J. *J. Mater. Chem.* **2009**, *19*, 5442–5451.
(45) Krebs, F. C.; Gevorgyan, S. A.; Gholamkhass, B.; Holdcroft, S.; Schlenker, C.; Thompson, M. E.; Thompson, B. C.; Olson, D.; Ginley, D. S.; Shaheen, S. E.; Alshareef, H. N.; Murphy, J. W.; Youngblood, W. J.; Heston, N. C.; Reynolds, J. R.; Jia, S.; Laird, D.; Tuladhar, S. M.; Dane, J. G. A.; Atienzar, P.; Nelson, J.; Kroon, J. M.; Wienk, M. M.; Janssen, R. A. J.; Tvingstedt, K.; Zhang, F.; Andersson, M.; Inganäs, O.; Lira-Cantu, M.; de Bettignies, R.; Guillerez, S.; Aernouts, T.; Cheyns, D.; Lutsen, L.; Zimmermann, B.; Würfel, U.; Niggemann, M.; Schleiermacher, H.-F.; Liska, P.; Grätzel, M.; Lianos, P.; Katz, E. A.; Lohwasser, W.; Jannon, B. *Sol. Energy Mater. Sol. Cells* **2009**, *93*, 1968–1977.

(46) Krebs, F. C. *Sol. Energy Mater. Sol. Cells* **2009**, *93*, 1636–1641.
(47) Winther-Jensen, B.; Krebs, F. C. *Sol. Energy Mater. Sol. Cells* **2006**, *90*, 123–132.
(48) Tvingstedt, K.; Inganäs, O. *Adv. Mater.* **2007**, *19*, 2893–2897.
(49) Strange, M.; Plackett, D.; Kaasgaard, M.; Krebs, F. C. *Sol. Energy Mater. Sol. Cells* **2008**, *92*, 805–813.
(50) Aernouts, T.; Vanlaeke, P.; Geens, W.; Poortmans, J.; Heremans, P.; Borghs, S.; Mertens, R.; Andriessen, R.; Leenders, L. *Thin Solid Films* **2004**, *451*−*452*, 22–25.
(51) Zimmermann, B.; Glatthaar, M.; Niggemann, M.; Riede, M. K.; Hinsch, A.; Gombert, A. *Sol. Energy Mater. Sol. Cells* **2007**, *91*, 374–378.
(52) Tromholt, T.; Gevorgyan, S. A.; Jørgensen, M.; Krebs, F. C.; Sylvester-Hvid, K. O. *ACS Appl. Mater. Interfaces* **2009**, *1*, 2768–2777.

AM900858X